

Eigenmode computations of frequency-dispersive photonic open structures: A non-linear eigenvalue problem.

Guillaume Demésy^{1,*}, André Nicolet¹, Boris Gralak¹, Christophe Geuzaine²,
Carmen Campos³, and Jose E. Roman³

¹CNRS, Aix-Marseille Université, Centrale Marseille, Institut Fresnel UMR 7249, 13013 Marseille, France.

²University of Liège, Dept. of Electrical Engineering and Computer Science, Montefiore Institute B28,
Quartier Polytech 1, Allée de la Découverte 10, B-4000 Liège, Belgium.

³Universitat Politècnica de València, D. Sistemes Informàtics i Computació, Camí de Vera, s/n, E-46022
València, Spain.

*Corresponding author : guillaume.demesy@fresnel.fr.

2022-03-02

Abstract

In this paper, we propose and compare different ways to address the numerical computation of the electromagnetic modes of frequency-dispersive scattering structures. A classical finite element formulation is derived for each proposed solution, which leads to a non-linear eigenvalue problem solved using recent adapted algorithms. The spectrum of a diffraction grating is computed for each approach. A necessary discussion of the corner issue with this sign-changing coefficient is provided. Various convergence aspects are addressed. Advantages and limitations of each solution are discussed.

1 Introduction

Modes are source free solutions of a propagation equation and contain all the information regarding the intrinsic resonances of a given structure. When dealing with the Helmholtz equation and frequency-dispersive media, the operator becomes eigenvalue dependent through the various relative permittivities and permeabilities of the materials. The EigenValue Problem (EVP) becomes non-linear.

For smooth and monotonic material dispersion relations, it is possible to think of an iterative process where one would set the permittivity, solve a linear EVP, adjust the permittivity value if necessary, and repeat the process hoping for reasonable convergence for a single eigenvalue. . . For more tormented dispersion relations, *i.e.* in the vicinity of a material intrinsic resonance, this simple iterative process is very likely to fail. For instance, a direct determination of the spectrum of a 3D gold nanoparticle embedded into a silicon background in the visible range is nowadays impossible.

Fortunately, the relative permittivity function can be accurately described as an analytical function of the frequency. The most famous models are the Drude, Lorentz, Debye models

[1], the so-called critical points [2] model or, in general, a rational function of the frequency [3]. . . In this framework, one can be more precise about the nature of our non linear EVP: It is a polynomial or rational EVP.

In this paper, we investigate various numerical scenarios to linearize this problem. We apply these approaches to an emblematic example in electromagnetism, the study of diffraction gratings. The dispersion relation of a grating is indeed the corner stone of its physical analysis.

The recent literature on modal analysis of such open structures, referred to as quasi-normal modes (QNM), is quite rich. Even if the question of completeness and orthogonality of the QNMs remains open theoretically, numerical quasi-normal modes expansion have been successfully used in various electromagnetic problems, allowing to explain in an elegant manner the resonant mechanisms of a structure and its excitation condition [4, 5]. Their application in nanophotonics can be found in Refs. [4, 6]. As described in the review article in Ref. [7], Some numerical approaches already address the problem of the non-linearity of the eigenvalue problem induced by frequency dispersion. A family of “pole search” methods [8, 9] allows to determine eigenvalues one by one by looking for poles of a scattering matrix into the complex plane. Another approach consists in computing the spectra corresponding to all possible values of the permittivity in a given frequency range and to post-interpolate the final spectrum [10]. Finally, extensions of Plane Wave Expansion (PWE) methods have been proposed [11, 12]. Nonetheless, getting the full spectrum in one single computation remains a harsh challenge. Given the spatial nature of the discretization when using Finite Elements (FE), the eigenvalue can be factorized until the final assembled matrix system. This fundamental aspect has a concrete consequence: It is possible to extract all the eigenvalues of the discrete system in one single computation. A Finite Difference Frequency Domain (FDFD) scheme leads to the same property and has been applied recently to open and dispersive electromagnetic structures [13, 14]. It relies on a square Yee grid. Finally, Boundary Elements (BE) have been used [15, 16] to calculate the QNMs of dispersive arbitrarily shaped yet homogeneous structures. Since the outgoing wave condition is handled via the Green’s function in this method, it depends on the eigenfrequency, and a contour integration has to be performed to find the poles of the scattering matrix.

In this paper, we propose to compare several Finite Element schemes to address the non-linear EVP arising from the frequency dispersion. The discrete problem is tackled using recent and efficient algorithms.

In the last decade, the numerical analysis community has made significant progress in the numerical solution of nonlinear eigenvalue problems, in understanding stability and conditioning issues, and also in proposing effective algorithms. Of particular interest for this paper are iterative methods for computing a few eigenvalues and corresponding eigenvectors of large-scale problems. This kind of methods have been developed for the case of polynomial eigenvalue problems [17, 18], but also for the more general nonlinear case [19]. The latter includes the rational eigenvalue problem, which is relevant for our purposes. Not only these methods have proved to be effective, but also some of them are available in the form of robust and efficient implementations in the SLEPc library [20]. With these new solvers, we can routinely compute the solution of problems with millions of unknowns using parallel computers. In this paper, we restrict to moderate problem sizes and hence parallel computing is not employed.

The paper is organized as follows. After recalling the equations at stake, five approaches to tackle the same problem are introduced. For each approach, a variational formulation is derived. In a second step, these formulations are benchmarked numerically using the state-of-the-art SLEPc solvers. The issues inherent to the sign-changing coefficients and corners is

discussed and the convergence of the fundamental mode of the structure is studied. Finally, a discussion on the respective strengths and limitations of all the solutions is conducted.

2 Problem statement

We are looking for the electromagnetic modes of 1D frequency-dispersive gratings, *i.e.* presenting one axis of invariance and one direction of periodicity. In non-conical mounts, we consider the two polarization cases referred to as *s-pol* (the electric field is along the axis of invariance) and *p-pol* (the magnetic field is along the axis of invariance, while the electric field is orthogonal to the axis of invariance). In this paper, the choice is made to focus on the more challenging *p-pol* case since the *s-pol* case is easier to tackle [21]. In particular, this polarization case leads to the surface plasmons and it is far more representative of the difficulties at stake in the general 3D case.

The relative permittivities of the constitutive materials are assumed to be frequency-dispersive. In other words, the photonic structure is fully described by the two periodic tensor fields, its relative permittivity $\boldsymbol{\varepsilon}_r(\mathbf{r}, \omega)$ and its relative permeability $\boldsymbol{\mu}_r(\mathbf{r})$, where $\mathbf{r} = (x, y)$.

In the *p-pol* case, we denote the relevant electromagnetic field components by $\mathbf{H} = h(\mathbf{r}) \mathbf{z}$ and $\mathbf{E} = E_x(\mathbf{r}) \mathbf{x} + E_y(\mathbf{r}) \mathbf{y}$. The traditional choice for the unknown in the 2D *p-pol* case is usually the out-of-plane magnetic field since it is then a scalar quantity. In absence of electromagnetic source, the resulting wave equation writes:

$$-\mu_{rzz}(\mathbf{r})^{-1} \operatorname{div} \left[\frac{\boldsymbol{\varepsilon}_r(\mathbf{r}, \omega)^T}{\det(\boldsymbol{\varepsilon}_r(\mathbf{r}, \omega))} \mathbf{grad} h \right] = \frac{\omega^2}{c^2} h. \quad (1)$$

This decoupling between the two *s/p*-polarization states is only possible for *z*-anisotropic media, where both the relative permittivity and permeability have the following form:

$$\boldsymbol{\varepsilon}_r = \begin{bmatrix} \varepsilon_{xx} & \varepsilon_a & 0 \\ \overline{\varepsilon_a} & \varepsilon_{yy} & 0 \\ 0 & 0 & \varepsilon_{zz} \end{bmatrix} \text{ and } \boldsymbol{\mu}_r = \begin{bmatrix} \mu_{xx} & \mu_a & 0 \\ \overline{\mu_a} & \mu_{yy} & 0 \\ 0 & 0 & \mu_{zz} \end{bmatrix}. \quad (2)$$

A less traditional choice consists in working with the in-plane electric field \mathbf{E} and the vector wave equation:

$$\boldsymbol{\varepsilon}_r(\mathbf{r}, \omega)^{-1} \mathbf{curl} [\boldsymbol{\mu}_r^{-1}(\mathbf{r}) \mathbf{curl} \mathbf{E}] = \frac{\omega^2}{c^2} \mathbf{E}. \quad (3)$$

However, what follows is meant to be extended straightforwardly to realistic 3D configurations, where vector fields/edge elements, just as in the 2D vector case, will be at stake. As a consequence, and even though this choice leads to larger problems at the discrete level due to the larger connectivity of edge elements, we choose this vector case as our reference problem.

Note that, given the location of the dispersive permittivity in the two wave equations above, it seems more reasonable at first glance to adopt the vector case where $\boldsymbol{\varepsilon}_r(\mathbf{r}, \omega)$ is outside the differential operator. As will be shown later, one can arbitrarily choose to consider \mathbf{E} or \mathbf{H} as the unknown of the problem under weak formulation. In fact, the scalar problem in Eq. (1) will be even solved as well for enlightening comparison purposes.

The above equations constitute eigenvalue problems where ω^2/c^2 appears as a possible eigenvalue of ω -dependent operators (explicitly $\boldsymbol{\varepsilon}_r(\mathbf{r}, \omega)^{-1} \mathbf{curl} [\boldsymbol{\mu}_r^{-1}(\mathbf{r}) \mathbf{curl} \cdot]$ in the general case) through the ω dependence of the relative permittivity. In other words, modal analysis of frequency-dispersive structures represents a non-linear eigenvalue problem.

3 Opto-geometric characteristics of the model

3.1 Geometry

The formalism presented in this paper is very general in the sense that the tensor fields $\varepsilon_r(\mathbf{r}, \omega)$ and $\mu_r(\mathbf{r})$ can be defined by part representing the various materials in the cell. Several dispersive materials can be considered, with arbitrarily high polynomial order. Graded-indexed and fully anisotropic materials can be handled as well.

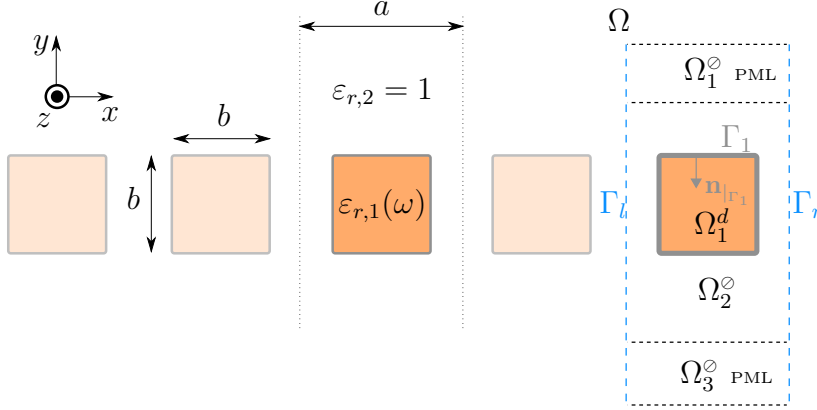


Figure 1: Geometry and notations of the problem.

In spite of the generality of the presented approach, for the sake of clarity, the derivations will be described in the frame of the example described in Fig. 1. We consider from now on a simple free-standing grating with a square section. Standard cartesian Perfectly Matched Layers (PMLs) are used to truncate infinite extensions of the domain. We denote the resulting bounded domain Ω , *i.e.* a closed subset of \mathbb{R}^2 , and its boundary $\partial\Omega$. The domain Ω can typically be constituted of several dispersive sub-domains with distinct frequency-dispersion relations (in this case, one single rod with support Ω_1^d of boundary Γ_1) and of several non-dispersive sub-domains. It is convenient to gather all the sub-domains ruled by the same dispersion regime together since they can be treated at once. All non-dispersive domains are denoted by $\Omega^\varnothing = \bigcup_i \Omega_i^\varnothing$. Finally, for each subset Ω_i , let \mathbf{l}_{Ω_i} be its characteristic function: $\mathbf{l}_{\Omega_i}(\mathbf{r}) = 1$ if $\mathbf{r} \in \Omega_i$ and $\mathbf{l}_{\Omega_i}(\mathbf{r}) = 0$ otherwise.

3.2 Material properties

The background is free-space (relative permittivity constant and equal to 1) and the rods are made of a Drude material. Their relative permittivity $\varepsilon_{r,1}$ writes classically [1]:

$$\varepsilon_{r,1}(\omega) = \varepsilon_\infty - \frac{\omega_d^2}{\omega(\omega + i\gamma_d)} \quad (4a)$$

$$= \frac{-\varepsilon_\infty(i\omega)^2 + \varepsilon_\infty\gamma_d(i\omega) - \omega_d^2}{-(i\omega)^2 + \gamma_d(i\omega)} \quad (4b)$$

$$:= \frac{\mathcal{N}_1(i\omega)}{\mathcal{D}_1(i\omega)}, \quad (4c)$$

where γ_d , ε_∞ and ω_d are real constants. It is important to note that the Drude model is causal and that $\varepsilon_{r,1}$ is a rational function of $(i\omega)$ with *real* coefficients (see Eq. (4b)). Finally, more realistic causal models than the Drude model have been found [3] and one can generally write $\varepsilon_{r,1}$ as a rational function (see Eq. (4c)). The generalization to a practical case with several frequency-dispersive domains Ω_i^d characterized by their permittivity $\varepsilon_{r,i}(\omega)$ fitted with an arbitrary rational function is straightforward:

$$\varepsilon_{r,i}(\omega) = \frac{\mathcal{N}_i(i\omega)}{\mathcal{D}_i(i\omega)} = \frac{\sum_{j=1}^{N_i} n_{i,j} (i\omega)^j}{\sum_{j=1}^{D_i} d_{i,j} (i\omega)^j}, \quad (5)$$

where $n_{i,j}$ and $d_{i,j}$ are real constants.

Finally, the unbounded nature of the problem is handled using PMLs. The reasons for this choice comes in twofold: (i) From the practical point of view, they allow to bound the computational domain (the complex change of variable is encoded into $\boldsymbol{\varepsilon}_r$ and $\boldsymbol{\mu}_r$ resulting in a semi-infinite layer that is eventually truncated), and (ii) from the theoretical point of view, PMLs allow to reveal [22] the so-called Quasi-Normal Modes (PMLs can be regarded as an analytic continuation in the complex plane). One could also think of a Sommerfeld radiation condition to handle this issue, but the resulting boundary term would be eigenvalue and space dependent.

Discussing the most appropriate PML parameters (*i.e.* damping profile) is outside the scope of this paper [23, 24], though it would be interesting to apply many of the results obtained in time and time-harmonic domains to the eigenvalue problem. The most simple constant complex stretch, ruled by the complex number $s_y = a + ib$ is used here. We introduce the complex PML tensor $\mathbf{S} = \text{Diag}(s_y, 1/s_y, s_y)$. One can eventually write the piecewise constant (in space) frequency-dispersive relative permittivity tensor of the problem as:

$$\boldsymbol{\varepsilon}_r(\mathbf{r}, \omega) = \begin{cases} \varepsilon_{r,1}(\omega) \mathbf{I} & \text{if } \mathbf{r} \in \Omega_1^d \\ \varepsilon_{r,2} \mathbf{I} & \text{if } \mathbf{r} \in \Omega_2^\circ \\ \varepsilon_{r,2} \mathbf{S} & \text{if } \mathbf{r} \in \Omega_1^\circ \cup \Omega_3^\circ \end{cases}. \quad (6)$$

The piecewise constant relative permeability tensor of the problem writes :

$$\boldsymbol{\mu}_r(\mathbf{r}) = \begin{cases} \mathbf{I} & \text{if } \mathbf{r} \in \Omega_1^d \cup \Omega_2^\circ \\ \mathbf{S} & \text{if } \mathbf{r} \in \Omega_1^\circ \cup \Omega_3^\circ \end{cases}. \quad (7)$$

Finally, Bloch-Floquet theorem is applied to the periodic structure. Our problem becomes parametrized by a positive real α which spans the reduced 1D Brillouin zone $[0, \pi/a]$ and, in return, we can restrict our study [25] to (a, α) quasi-periodic solutions (eigenvectors) of the form $\mathbf{E} = \mathbf{E}_\# e^{i\alpha x}$, where $\mathbf{E}_\#$ is a a -periodic vector field.

3.3 Function spaces

Several function spaces are needed to formulate the different approaches of the problem.

Concerning the p -pol vector case described in Eq. (3), Bloch conditions are applied on lateral boundaries $\Gamma_l \cup \Gamma_r$. If infinite perfectly matched layers are the appropriate theoretical tool to reveal the quasi-normal modes by rotating the continuous spectrum into the complex plane, they have to be truncated in practice. The truncation discretizes the rotated continuous

spectrum and one can choose to apply Dirichlet or Neumann boundary conditions, resulting in a slightly different discretization [22]. We choose homogeneous Dirichlet conditions on $\Gamma_b \cup \Gamma_t$, which at least decreases the number of unknowns. With this in mind, let us define the following Sobolev space of (a, α) quasi-periodic vector fields vanishing on $\Gamma_b \cup \Gamma_t$:

$$\mathcal{H}_{\alpha,0}(\Omega, \mathbf{curl}) = \left\{ \mathbf{E} \in (L^2)^2 : \mathbf{curl} \mathbf{E} \in (L^2)^2, \mathbf{E}|_{\Gamma_r} = e^{i\alpha a} \mathbf{E}|_{\Gamma_l} \text{ and } \mathbf{E}|_{\Gamma_b} = \mathbf{E}|_{\Gamma_t} = \mathbf{0} \right\}. \quad (8)$$

The same considerations apply to the p -pol scalar case described in Eq. (1). However, in order to keep the same discretization of the continuous spectrum, we apply homogeneous Neumann conditions on $\Gamma_b \cup \Gamma_t$. With this in mind, let us define the following Sobolev space of (a, α) quasi-periodic scalar fields:

$$\mathcal{H}_\alpha(\Omega, \mathbf{grad}) = \left\{ h \in L^2 : \mathbf{grad} h \in L^2, h|_{\Gamma_r} = e^{i\alpha a} h|_{\Gamma_l} \text{ and } \mathbf{grad} h \cdot \mathbf{n}|_{\Gamma_b} = \mathbf{grad} h \cdot \mathbf{n}|_{\Gamma_t} = 0 \right\}. \quad (9)$$

4 Dealing with the eigenvalue problem non-linearity

4.1 A physical linearization via auxiliary fields (Aux-E case)

The problem is reformulated using auxiliary physical fields [26, 27], as detailed in our previous work in Ref. [21]. The procedure to obtain this extension of the Maxwell's classical operator is briefly recalled here. By defining an auxiliary field [28] for each resonance (pole) of the permittivity that couples with classical electromagnetic fields, one can extend and linearize the classical Maxwell operator. In the present case of a simple Drude model recalled in Eq. (4a), a single auxiliary field denoted \mathbf{A}_1^d is required, and defined in frequency-domain as:

$$\mathbf{A}_1^d(\mathbf{r}, t) = -2i \frac{\omega_d}{\sqrt{2}} \int_{-\infty}^t \exp[-\gamma_d(t-s)] \mathbf{E}(\mathbf{r}, s) ds. \quad (10)$$

This auxiliary field \mathbf{A}_1^d has for spatial support Ω_1^d and satisfies natural boundary conditions on Γ_1 . It belongs to $\mathcal{H}(\Omega_1^d, \mathbf{curl})$. An intermediate frequency-dispersion free permittivity tensor field $\epsilon_r^\circ(\mathbf{r})$ is convenient here:

$$\epsilon_r^\circ(\mathbf{r}) = \begin{cases} \epsilon_\infty \mathbf{I} & \text{if } \mathbf{r} \in \Omega_1^d \\ \epsilon_{r,2} \mathbf{I} & \text{if } \mathbf{r} \in \Omega_2^\circ \\ \epsilon_{r,2} \mathbf{S} & \text{if } \mathbf{r} \in \Omega_1^\circ \cup \Omega_3^\circ \end{cases}. \quad (11)$$

In matrix form, the following linear eigenvalue problem is obtained:

$$\mathbf{M}(\mathbf{r}) \mathcal{U}(\mathbf{r}, \omega) = \omega \mathcal{U}(\mathbf{r}, \omega), \quad (12)$$

where

$$\mathbf{M}(\mathbf{r}) = \begin{bmatrix} 0 & i(\epsilon_0 \epsilon_r^\circ)^{-1} \mathbf{curl} \cdot & \frac{\omega_d}{\sqrt{2}} \epsilon_r^{\circ-1} \\ -i(\mu_0 \boldsymbol{\mu}_r)^{-1} \mathbf{curl} \cdot & 0 & 0 \\ 2 \frac{\omega_d}{\sqrt{2}} & 0 & -i\gamma_d \end{bmatrix} \text{ and } \mathcal{U}(\mathbf{r}, \omega) = \begin{bmatrix} \mathbf{E}(\mathbf{r}, \omega) \\ \mathbf{H}(\mathbf{r}, \omega) \\ \mathbf{A}_1^d(\mathbf{r}, \omega) \end{bmatrix}. \quad (13)$$

Note that when discretizing the problem using Finite Elements, the electric field and magnetic field cannot be represented on the same edges. The former should be discretized on the dual basis of the latter. However, the basis functions associated with the dual unstructured FEM mesh are not easy to construct. A possible workaround would consist in working with face elements and the 2-form \mathbf{B} instead of edge elements and the 1-form \mathbf{H} . Alternatively, in this paper, we classically chose to get rid of \mathbf{H} . The cost is that a quadratic eigenproblem is obtained whereas the system in Eq. (13) was linear:

$$\omega^2 \mathbf{M}_2(\mathbf{r}) \mathcal{V}(\mathbf{r}, \omega) + \omega \mathbf{M}_1(\mathbf{r}) \mathcal{V}(\mathbf{r}, \omega) + \mathbf{M}_0(\mathbf{r}) \mathcal{V}(\mathbf{r}, \omega) = \mathbf{0}, \quad (14)$$

where:

$$\mathbf{M}_2 = \begin{bmatrix} -\boldsymbol{\varepsilon}_r^\circ & 0 \\ 0 & 0 \end{bmatrix}, \mathbf{M}_1 = \begin{bmatrix} 0 & \frac{\omega_d}{\sqrt{2}} \\ 0 & -1 \end{bmatrix}, \mathbf{M}_0 = \begin{bmatrix} c^2 \mathbf{curl} [\boldsymbol{\mu}_r^{-1} \mathbf{curl} \cdot] & 0 \\ 2 \frac{\omega_d}{\sqrt{2}} & -i\gamma_d \end{bmatrix}, \text{ and } \mathcal{V}(\mathbf{r}, \omega) = \begin{bmatrix} \mathbf{E} \\ \mathbf{A}_1^d \end{bmatrix}. \quad (15)$$

Finally, this quadratic eigenvalue problem writes under variational form:

$$\left| \begin{array}{l} \text{Given } \alpha \in [0, \pi/a], \text{ find } (\omega, [\mathbf{E}, \mathbf{A}_1^d]^T) \in \mathbb{C} \times [\mathcal{H}_{\alpha,0}(\Omega, \mathbf{curl}) \times \mathcal{H}(\Omega_1^d, \mathbf{curl})] \text{ such that:} \\ \forall \mathcal{W} = [\mathbf{W}, \mathbf{W}_a] \in \mathcal{H}_{\alpha,0}(\Omega, \mathbf{curl}) \times \mathcal{H}(\Omega_1^d, \mathbf{curl}), \\ \omega^2 \int_{\Omega} (\mathbf{M}_2 \mathcal{V}) \overline{\mathcal{W}} d\Omega + \omega \int_{\Omega} (\mathbf{M}_1 \mathcal{V}) \overline{\mathcal{W}} d\Omega + \int_{\Omega} (\mathbf{M}_0 \mathcal{V}) \overline{\mathcal{W}} d\Omega = 0. \end{array} \right. \quad (16)$$

This linearization can be described as a physical one since, unlike the purely numerical ones in the following, a larger system is obtained with extra unknowns *inside the dispersive element solely*. In this simplified version of the auxiliary fields theory called the resonance formalism, the auxiliary field fulfills a simple relation with the polarization vector: $\partial_t \mathbf{P}(\mathbf{r}, t) = i\epsilon_0 \frac{\omega_d}{\sqrt{2}} \mathbf{A}_1^d(\mathbf{r}, t)$. This approach is identical to the one presented by Fan *et al.* in Ref. [29]. It is also very similar to the treatment of frequency-dispersive media made in time domain methods for direct problems such as FDTD [30].

In the following, the case described in Eq. (16) will be referred to as the Aux-E case.

4.2 Electric field polynomial eigenvalue problem (PEP-E and NEP-E cases)

In this section, a purely numerical linearization is considered. This approach begins with writing the eigenvalue problem Eq. (3) under its variational form:

$$\left| \begin{array}{l} \text{Given } \alpha \in [0, \pi/a], \text{ find } (\omega, \mathbf{E}) \in \mathbb{C} \times \mathcal{H}_{\alpha,0}(\Omega, \mathbf{curl}) \text{ such that:} \\ \forall \mathbf{W} \in \mathcal{H}_{\alpha,0}(\Omega, \mathbf{curl}), \\ - \int_{\Omega} \boldsymbol{\mu}_r^{-1} \mathbf{curl} \mathbf{E} \cdot \overline{\mathbf{curl} \mathbf{W}} d\Omega + \frac{\omega^2}{c^2} \int_{\Omega} \boldsymbol{\varepsilon}_r^{-1} \mathbf{E} \cdot \overline{\mathbf{W}} d\Omega = 0. \end{array} \right. \quad (17)$$

Note that the boundary term on periodic lines Γ_r and Γ_l vanishes due to opposite signs of normals [31].

Then, recalling that the whole domain Ω can be split into frequency-dispersive domains (Ω_1^d solely in this simplified case) and non dispersive domains Ω° , and that the permittivity

tensor is a constant by part tensor field of \mathbf{r} , our problem becomes :

$$\left| \begin{array}{l} \text{Given } \alpha \in [0, \pi/a], \text{ find } (\omega, \mathbf{E}) \in \mathbb{C} \times \mathcal{H}_{\alpha,0}(\Omega, \mathbf{curl}) \text{ such that:} \\ \forall \mathbf{W} \in \mathcal{H}_{\alpha,0}(\Omega, \mathbf{curl}), \\ - \int_{\Omega} \mu_r^{-1} \mathbf{curl} \mathbf{E} \cdot \overline{\mathbf{curl} \mathbf{W}} d\Omega \\ + \frac{\omega^2}{c^2} \int_{\Omega} \epsilon_r \mathbf{E} \cdot \overline{\mathbf{W}} d\Omega + \frac{\omega^2}{c^2} \frac{\mathcal{N}_1(i\omega)}{\mathcal{D}_1(i\omega)} \int_{\Omega} \mathbf{E} \cdot \overline{\mathbf{W}} d\Omega = 0. \end{array} \right. \quad (18)$$

A last mere multiplication by $\mathcal{D}_1(i\omega)$ allows to put our problem under the form of a polynomial eigenvalue problem:

$$\left| \begin{array}{l} \text{Given } \alpha \in [0, \pi/a], \text{ find } (\omega, \mathbf{E}) \in \mathbb{C} \times \mathcal{H}_{\alpha,0}(\Omega, \mathbf{curl}) \text{ such that:} \\ \forall \mathbf{W} \in \mathcal{H}_{\alpha,0}(\Omega, \mathbf{curl}), \\ - \mathcal{D}_1(i\omega) \int_{\Omega} \mu_r^{-1} \mathbf{curl} \mathbf{E} \cdot \overline{\mathbf{curl} \mathbf{W}} d\Omega \\ + \frac{\omega^2}{c^2} \mathcal{D}_1(i\omega) \int_{\Omega} \epsilon_r \mathbf{E} \cdot \overline{\mathbf{W}} d\Omega + \frac{\omega^2}{c^2} \mathcal{N}_1(i\omega) \int_{\Omega} \mathbf{E} \cdot \overline{\mathbf{W}} d\Omega = 0. \end{array} \right. \quad (19)$$

The Drude permittivity model has a pole in zero, leading to a polynomial EVP of order 3. Otherwise, when considering one single frequency-dispersive material, the final order will be $2 + \text{Deg}(\mathcal{D}_i)$. More generally, note that the final degree of the polynomial EVP is $2 + \sum_{i=1}^N \text{Deg}(\mathcal{D}_i)$ in the case of N (distinct) frequency-dispersive materials.

In the following, the approaches described in Eq. (19) and Eq. (18) will be referred to as the PEP-E and NEP-E approaches respectively. They differ by the type of solver used for their numerical treatment as detailed later.

4.3 Electric field polynomial eigenvalue problem with Lagrange multipliers (Lag-E case)

From the beginning of the discussion, it is tempting to consider the polynomial eigenvalue problem under its strong form, and directly multiply our propagation equation by the denominator of the frequency-dispersive permittivity. Recalling that the relative permittivity tensor field is defined by part in each domain, we obtain:

$$\left(\mathbf{l}_{\Omega^{\circ}}(\mathbf{r}) + \mathcal{D}_1(i\omega) \mathbf{l}_{\Omega_1^d}(\mathbf{r}) \right) \mathbf{curl} [\mu_r^{-1}(\mathbf{r}) \mathbf{curl} \mathbf{E}] = \left(\epsilon_r(\mathbf{r}) \mathbf{l}_{\Omega^{\circ}} + \mathcal{N}_1(i\omega) \mathbf{l}_{\Omega_1^d}(\mathbf{r}) \right) \frac{\omega^2}{c^2} \mathbf{E}. \quad (20)$$

Terms of the form $[f(\mathbf{r}) \mathbf{curl} \mu_r^{-1} \mathbf{curl} \mathbf{E}]$ are obtained, where f is a constant by part complex scalar function. The weak formulation is not classical, since after multiplication by a test function \mathbf{W} and integration over Ω , we obtain in the sense of distributions :

$$\begin{aligned} \int_{\Omega} [f(\mathbf{x}) \mathbf{curl} \mu_r^{-1} \mathbf{curl} \mathbf{E}] \cdot \overline{\mathbf{W}} d\Omega &= \int_{\Omega} f(\mathbf{x}) \mu_r^{-1} \mathbf{curl} \mathbf{E} \cdot \mathbf{curl} \overline{\mathbf{W}} d\Omega \\ &- \int_{\partial\Omega} f(\mathbf{x}) \mu_r^{-1} \mathbf{curl} \mathbf{E} \cdot [\mathbf{n}_{|\partial\Omega} \times \overline{\mathbf{W}}] d\Gamma \\ &+ \int_{\Gamma_1} f_{\text{jump}}^{\circ \rightarrow d} \left[[\mu_r^{-1} \mathbf{curl} \mathbf{E}] \times \mathbf{n}_{|\Gamma_1} \right] \cdot \overline{\mathbf{W}} d\Gamma. \end{aligned} \quad (21)$$

In other words, the two first terms in the right hand side of Eq. (21) look exactly like the traditional integration by part, pondered by f . As for the last term, it represents a jump to be imposed to the quantity $[\boldsymbol{\mu}_r^{-1} \text{curl} \mathbf{E}] \times \mathbf{n}_{|\Gamma_1}]$, which is nothing but the tangential trace of \mathbf{H} on Γ_1 . This quantity can be tuned via the adjunction of a Lagrange multiplier. In other words, the goal is here to split the problem into groups ruled by the same frequency dispersion law, and to introduce an extra unknown in order to reassemble the different groups satisfying the appropriate jump conditions. Thus, the problem is split into two distinct parts and two fields \mathbf{E}_1 and \mathbf{E}_2 are defined, with respective support Ω_1^d and Ω° . A Lagrange multiplier $\boldsymbol{\lambda}$ is introduced on Γ_1 in order to set the appropriate boundary conditions. The variational form of the eigenproblem writes:

$$\left| \begin{array}{l} \text{Given } \alpha \in [0, \pi/a], \\ \text{find } (\omega, (\mathbf{E}_1, \mathbf{E}_2, \boldsymbol{\lambda})) \in \mathbb{C} \times [\mathcal{H}(\Omega_1^d, \text{curl}) \times \mathcal{H}_{\alpha,0}(\Omega^\circ, \text{curl}) \times \mathcal{H}(\Gamma_1, \text{curl})] \text{ such that:} \\ \forall [\mathbf{W}_1, \mathbf{W}_2, \boldsymbol{\nu}]^T \in \mathcal{H}(\Omega_1^d, \text{curl}) \times \mathcal{H}_{\alpha,0}(\Omega^\circ, \text{curl}) \times \mathcal{H}(\Gamma_1, \text{curl}), \\ \mathcal{D}_1(i\omega) \int_{\Omega} \boldsymbol{\mu}_r^{-1} \text{curl} \mathbf{E}_1 \cdot \overline{\text{curl} \mathbf{W}_1} d\Omega \\ + \frac{\omega^2}{c^2} \mathcal{N}_1(i\omega) \int_{\Omega} \mathbf{E}_1 \cdot \overline{\mathbf{W}_1} d\Omega + \mathcal{D}_1(i\omega) \int_{\Gamma} \boldsymbol{\lambda} \cdot \overline{\mathbf{W}_1} d\Gamma = 0 \\ \text{and} \\ \int_{\Omega} \boldsymbol{\mu}_r^{-1} \text{curl} \mathbf{E}_2 \cdot \overline{\text{curl} \mathbf{W}_2} d\Omega \\ + \frac{\omega^2}{c^2} \int_{\Omega} \boldsymbol{\epsilon}_r^\circ \mathbf{E}_2 \cdot \overline{\mathbf{W}_2} d\Omega - \int_{\Gamma} 1 \boldsymbol{\lambda} \cdot \overline{\mathbf{W}_2} d\Gamma = 0 \\ \text{and} \\ \int_{\Gamma} (\mathbf{E}_1 - \mathbf{E}_2) \cdot \overline{\boldsymbol{\lambda}} d\Gamma = 0. \end{array} \right. \quad (22a)$$

$$\begin{aligned} & \mathcal{D}_1(i\omega) \int_{\Omega} \boldsymbol{\mu}_r^{-1} \text{curl} \mathbf{E}_1 \cdot \overline{\text{curl} \mathbf{W}_1} d\Omega \\ & + \frac{\omega^2}{c^2} \mathcal{N}_1(i\omega) \int_{\Omega} \mathbf{E}_1 \cdot \overline{\mathbf{W}_1} d\Omega + \mathcal{D}_1(i\omega) \int_{\Gamma} \boldsymbol{\lambda} \cdot \overline{\mathbf{W}_1} d\Gamma = 0 \end{aligned} \quad (22b)$$

and

$$\begin{aligned} & \int_{\Omega} \boldsymbol{\mu}_r^{-1} \text{curl} \mathbf{E}_2 \cdot \overline{\text{curl} \mathbf{W}_2} d\Omega \\ & + \frac{\omega^2}{c^2} \int_{\Omega} \boldsymbol{\epsilon}_r^\circ \mathbf{E}_2 \cdot \overline{\mathbf{W}_2} d\Omega - \int_{\Gamma} 1 \boldsymbol{\lambda} \cdot \overline{\mathbf{W}_2} d\Gamma = 0 \end{aligned} \quad (22c)$$

and

$$\int_{\Gamma} (\mathbf{E}_1 - \mathbf{E}_2) \cdot \overline{\boldsymbol{\lambda}} d\Gamma = 0. \quad (22d)$$

In the system Eqs. (22), we clearly recognize into the two first equations Eqs. (22b, 22c), apart from their respective last boundary term, the wave equation in the dispersive domain Ω_1^d (Eq. (22b)) and in the non-dispersive domain Ω° . As for this last boundary term, it accounts for the discontinuity of the denominator of the permittivity over Ω through the Lagrange multiplier $\boldsymbol{\lambda}$ by imposing appropriate jumps to the normal derivative of \mathbf{E} . Finally, the continuity of the tangential component of $\mathbf{E} = \mathbf{E}_1 + \mathbf{E}_2$ on Γ_1 is restored (Eq. (22d)).

The advantage of this approach is that, in case of several dispersive materials, the degree of the final polynomial EVP will remain the maximum degree of the polynomials \mathcal{D}_i instead of the sum of the degrees the \mathcal{D}_i polynomials as in Sec. 4.2. However, in this example where a Drude material is in contact with a dispersion-free region, it results in a 3^{rd} order polynomial as in the PEP-E approach. Note that one drawback is the additional surface unknowns introduced by the Lagrange multipliers.

In the following, the approach described by Eqs. (22b, 22c, 22d) will be referred to as the Lag-E approach.

4.4 Magnetic field polynomial eigenvalue problem (PEP-h case)

For reference and comparison, we will also solve here the scalar problem corresponding to Eq. (1). Let us recall that homogeneous Neumann boundary conditions are imposed at the extremities of the PMLs in order to keep the same discretization of the continuous spectrum as in the other approaches based on the electric field. As for discretization, this continuous problem can be tackled using nodal elements whereas the previous ones requires edge elements. The same considerations as in the previous vector case allow to establish the eigenproblem for the scalar unknown h :

$$\left| \begin{array}{l} \text{Given } \alpha \in [0, \pi/a], \text{ find } (\omega, h) \in \mathbb{C} \times \mathcal{H}_{\alpha,0}(\Omega, \mathbf{grad}) \text{ such that:} \\ \forall w \in \mathcal{H}_{\alpha,0}(\Omega, \mathbf{grad}), \\ - \mathcal{D}_1(i\omega) \int_{\Omega_1} \mathbf{grad} h \cdot \overline{\mathbf{grad} w} d\Omega_1 \\ - \mathcal{N}_1(i\omega) \int_{\Omega_2} \frac{\boldsymbol{\epsilon}_r(\mathbf{r})^T}{\det(\boldsymbol{\epsilon}_r(\mathbf{r}))} \mathbf{grad} h \cdot \overline{\mathbf{grad} w} d\Omega_2 \\ + \frac{\omega^2}{c^2} \mathcal{N}_1(i\omega) \int_{\Omega} \mu_{rzz} h \cdot \overline{w} d\Omega = 0. \end{array} \right. \quad (23)$$

It results in our example in a 4th order polynomial EVP.

In the following, the approach described in Eq. (23) will be referred to as the PEP-h approach.

5 Numerical results

5.1 Discretization and sum up

The structure described in Fig. 1 was meshed using the GNU software Gmsh [32]. An example of mesh is shown in Fig. 2. The mesh size is set to a/N in Ω_2° (free-space), $a/(3N)$ in and around Ω_1^d (dispersive rod), where N is set to an integer value. First or second order edge elements (or Webb elements with interpolation order $k = 1$ or 2 [33, 34]) are used in electric field cases (Aux-E, PEP-E, NEP-E, Lag-E) and first or second order nodal elements are used in the magnetic field case (PEP-h) depending on the study. The GetDP [35] software allows to handle the various required basis functions handily. The different cases and their main differences (unknown field, polynomial orders, number of DOFs for a particular mesh, solver used...) are summed up in Table 1.

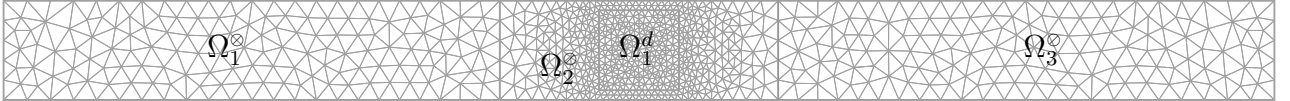


Figure 2: Mesh of the computational domain for $N = 5$. The mesh size is set to a/N in Ω_2° (free-space), $a/(3N)$ in and around Ω_1^d (dispersive rod).

5.2 Solvers

Very recent progress in sparse matrix eigenvalue solvers allow to tackle the discrete problem very efficiently. For the purpose of this study, we interfaced GetDP with two particularly

well suited and recent solvers of the SLEPc library [20] dedicated to solve large scale sparse eigenvalue problems. Depending on the eigenproblem, GetDP can call linear, quadratic, general polynomial, or rational eigenvalue solvers of SLEPc.

Concerning the auxiliary field (Aux-E) formulation, all is needed is a solver adapted to quadratic eigenproblems. Again, that is the particularity of this physical linearization, one can add more poles to the permittivity rational function or more dispersive materials: It will only result in defining new auxiliary fields in the elements leading to a larger system that will remain quadratic.

As for the polynomial eigenproblems (PEP-E, Lag-E, PEP-h) described in Eqs. (19,22,23), the matrices corresponding to the various powers of ω (that is, in our example, 4 matrices for the electric field formulations and 5 for the magnetic electric field formulation) are assembled separately in GetDP and simply passed to SLEPc. SLEPc provides a PEP module for the solution of polynomial eigenvalue problems, either quadratic or of higher degree d . The user can choose among several solvers. Most of these solvers are based on linearization, meaning that internally a linear eigenvalue problem is built somehow and solved with more traditional linear eigensolvers. The linear eigenproblem produced by the linearization is of dimension $d \cdot n$, where n is the size of the polynomial problem. Hence, a naive implementation of the linearization is going to require d times as much memory with respect to the linear case. The default SLEPc polynomial solver, named TOAR, is memory-efficient because it represents the subspace basis in a compact way, $V = (I_d \otimes U)G$, where vectors of the basis U have length n as opposed to length $d \cdot n$ for vectors of V . The TOAR algorithm builds a Krylov subspace with this basis structure, and it has been shown to be numerically stable [36]. Apart from the memory savings, the method is cheaper in terms of computations compared to operating with the explicitly formed linearization. In particular, when performing the shift-and-invert spectral transformation for computing eigenvalues close to a given target value in the complex plane, it is not necessary to factorize a matrix of order $d \cdot n$ but a matrix of order n instead. SLEPc's solvers also incorporate all the necessary ingredients for making the method effective and accurate, such as scaling, restart, eigenvalue locking, eigenvector extraction, and iterative refinement, as well as parallel implementation. All the details can be found in [37].

Table 1: A synthetic view of all the presented approaches.

Name	Aux-E	PEP-E	NEP-E	Lag-E	PEP-h
Formulation	Eq. (16)	Eq. (19)	Eq. (18)	Eq. (22)	Eq. (23)
Unknown(s)	$\mathbf{E}, \mathbf{A}_1^d$	\mathbf{E}	\mathbf{E}	$\mathbf{E}_1, \mathbf{E}_2, \boldsymbol{\lambda}$	h
Element type	Edge	Edge	Edge	Edge	Nodal
Polynomial order	2	3	- (rational)	3	4
SLEPc solver	PEP (Quadratic)	PEP	NEP	PEP	PEP
number of DOFs for $N = 15$ and first order FE	44270	33346	33346	33938	22274
number of eigenvalues out of 500 / $\varepsilon_{r,2}(\omega) = 0$	118 ± 7	120 ± 6	121 ± 6	119 ± 8	129 ± 4

The rational eigenproblem described in Eq. (18) is even simpler since SLEPc now has a built-in solver class to handle complex rational functions. As a result, one can directly provide

the 3 necessary matrices corresponding to the tree terms in Eq. (18), along with the desired dispersive relative permittivity function. Note that for several dispersive domains with distinct materials with a high number of poles, the product of all the involved denominators in the polynomial approach (Eq. (19)) would be tedious to write. However, the number of terms to write with the NEP solvers remains “two plus the number of distinct dispersive media”. We present both these twin approaches, but, from the practical point of view, the rational NEP solver class is clearly the best match for our needs.

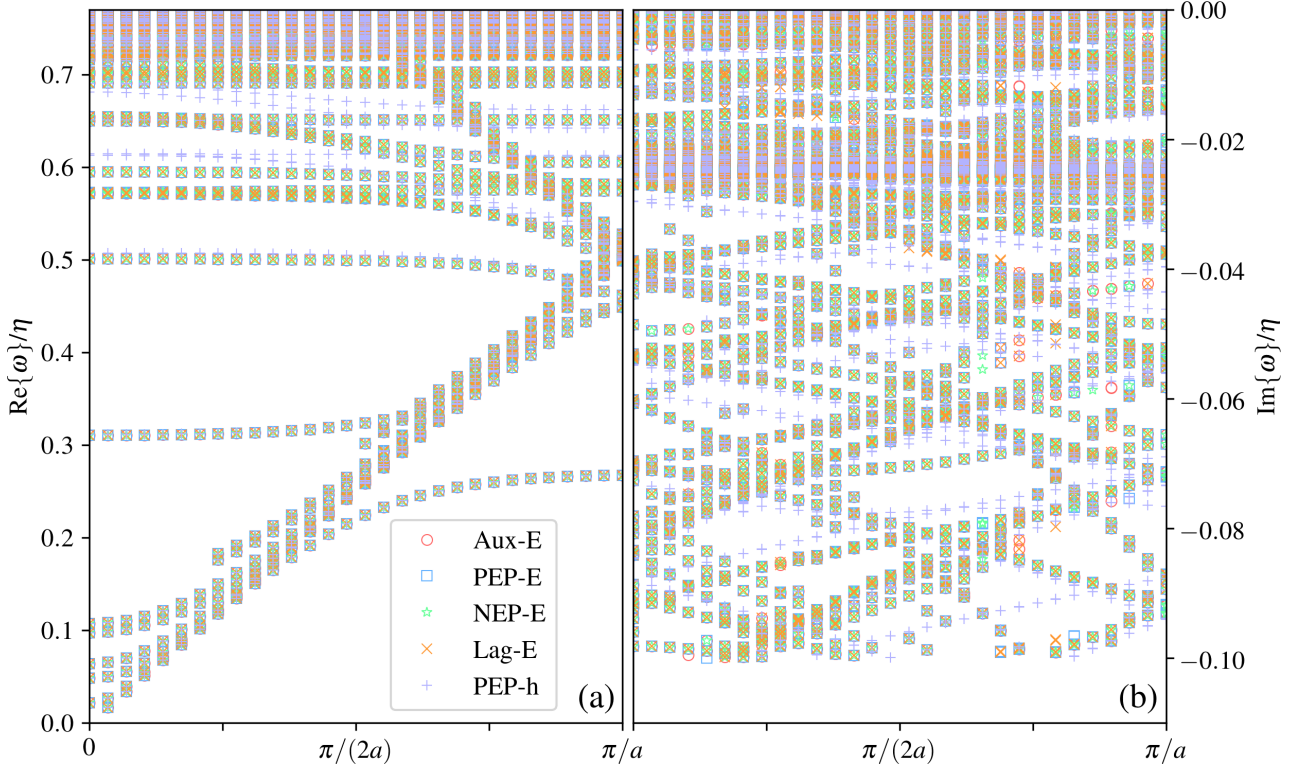


Figure 3: (a) Real and (b) imaginary parts of the normalized eigenvalues ($\eta = \frac{2\pi c}{a}$) as a function of the Bloch variable α for the five methods.

SLEPc’s NEP module for general nonlinear eigenproblems [38] can be used to compute a few eigenvalues (and corresponding eigenvectors) of any eigenproblem that is nonlinear with respect to the eigenvalue (not the eigenvector). This includes the rational eigenvalue problem, for which SLEPc solvers provide specific support. The problem is expressed in the form

$$\sum_{i=0}^{\ell-1} A_i f_i(\lambda) x = 0, \quad (24)$$

where A_i are the matrix coefficients and $f_i(\cdot)$ are nonlinear functions. Again, SLEPc provides a collection of solvers from which the user can select the most appropriate one. Particularly interesting are the methods based on approximation followed by linearization. An example of such methods is the interpolation solver, that approximates the nonlinear function by the interpolation polynomial in a given interval, and then uses the PEP module to solve the resulting polynomial eigenproblem. This approach is available only for the case of real eigenvalues and hence cannot be applied in our case. A similar strategy is used in the NLEIGS algorithm [39], that builds a rational interpolation which in turn is linearized to get a linear eigenvalue

problem. As opposed to the case of the polynomial eigenproblem, in this case the dimension of the linearized problem is not known a priori, since the number of terms depends on the function being interpolated. NLEIGS determines the number of terms based on a tolerance for interpolation. In a general nonlinear function, the user must provide a discretization of the singularity set, but in the case that the nonlinear eigenproblem is itself rational, this is not necessary and SLEPc automatically builds an exact rational interpolation of size equal to the number of poles (plus the polynomial part if present). Once the rational interpolation is obtained, the last step is to create a memory-efficient Krylov expansion associated with the linearization, in a similar way as in polynomial problems, without explicitly building the matrix of the linearization and representing the Krylov basis in a compact way. This is the approach that has been used in this paper for the NEP-E formulation.

5.3 Spectrum of the structure

The numerical values used in Refs. [8, 40] in the case of 2D photonic crystals are considered here:

$$\varepsilon_\infty = 1, \quad \gamma_d = 0.05\eta, \quad \text{and } \omega_d = 1.1\eta, \quad \text{with } \eta = \frac{2\pi c}{a}. \quad (25)$$

The square rod section is set to $b = 0.806a$, the PML thickness to $5a$ and the space between the rods and the PMLs to a . For the spectrum computed in this section, the average mesh size is set to a/N in Ω_2° (free space), $a/(3N)$ in and around Ω_1^d (dispersive rod), with $N = 15$. A coarse version of the mesh is shown in Fig. 2 with $N = 5$. First order Finite Element interpolation is used. Note that this choice is arbitrary in the sense that one cannot choose the mesh size like in time-harmonic direct problems where the time frequency is fixed, and thus the spatial frequencies of the unknown field inside each domain are known in advance. The unknown is precisely the time frequency and moreover, in this dispersive case, the expected spatial variations of the corresponding eigenvectors can tend towards zero in some parts of the complex plane. For instance, we expect an accumulation point [21] around the locus ω satisfying $\varepsilon_{r,1}(\omega) = -1$, which corresponds to all surface plasmon modes supported around the rod.

A traditional representation of the spectrum of such a 1D periodic structure is given in Fig. 3(a), this is the so-called dispersion relation of the grating. For each formulation, the reduced Brillouin zone $[0, \pi/a]$ is spanned (30 points) and 500 complex eigenvalues are computed. In lossless 1D systems such as infinite thin films, the spectrum is real. However, due to both radiation and Joule losses, all the eigenvalues are complex and their imaginary parts is given in Fig. 3(b). The numerical agreement between all electric field based approaches is striking.

In this figure, we retrieve easily the periodic free-space continuous spectrum forming the folded light line, which corresponds to PML modes. Just below the first branch of the folded light line, the shape of the line corresponding to the lowest (fundamental) eigenfrequency supported by the grating is characteristic [41, 42, 43] of this type of structure. The real part of one eigenvector, or mode, of this particular line is shown in Fig. 7(f) for $\alpha = 3\pi/(4a)$.

Our region of interest of the complex frequency plane (lower right quarter) exhibits several very particular and unavoidable points.

The first one corresponds to the zeros of the dispersive permittivity $\varepsilon_{r,1}$. With our Drude model, the present region of interest exhibits a single zero shown in Figs. 4-5 by a large black cross. When reaching a zero of $\varepsilon_{r,1}$, the divergence condition $\text{div } \boldsymbol{\varepsilon}_r \mathbf{E} = 0$ fails and \mathbf{E} can take

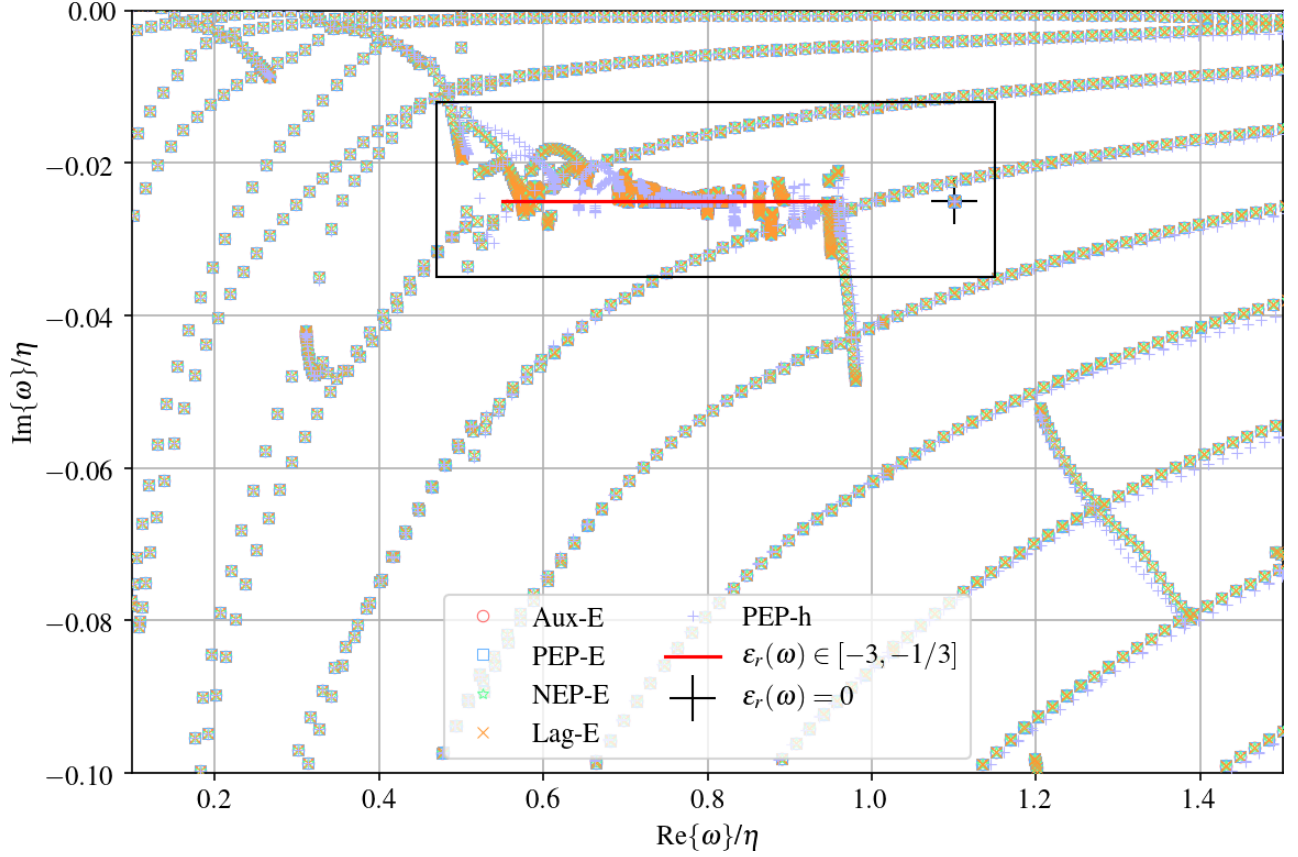


Figure 4: Same numerical set of eigenvalues as depicted in Fig. 3 represented in the complex plane: The reduced Brillouin zone is spanned from 0 to π/a with 30 points. This representation highlights the discrepancies between the magnetic and the electric field formulations, noticeable inside the solid black rectangle). The critical interval of complex frequencies due to sharp corners is represented by the red solid line. The black cross represents the relevant zero of $\varepsilon_{r,1}$.

any value. As shown in the last line of Tab. 1, for each of the 30 EVPs solved to compute the dispersion relation with 500 requested eigenvalues, approximately one fourth of them actually correspond to zeros of the permittivity, which is of course an important limitation in terms of computation time. Note that since these points are known in advance, a numerical workaround would consist in adding some exclusion regions of the complex plane via the SLEPc region class. This problem does not happen in the s -pol case where the only unknown is E_z since 2D nodal elements are divergence free by construction ($\partial_x E_x = \partial_y E_y = \partial_z E_z = 0$). One reason for solving the p -pol case using the PEP-h was to check whether the impact of problem could be reduced using the magnetic field unknown. As shown in the last column of Tab. 1, it is not the case.

Looking more closely at Figs. 3(a)-(b), we notice a discrepancy between the electric field formulations (Aux-E, PEP-E, NEP-E, Lag-E) and the only magnetic field formulation (PEP-h). For further investigation, another representation of the spectrum is adopted: All the computed eigenvalues are shown in the complex plane in Fig. 4 for all the computed values of the Bloch variable α . The data being the same as in Figs. 3(a)-(b), the overall agreement still holds but the discrepancy between the vector electric field formulations and the magnetic one appears more clearly within the black solid line rectangle frame. A zoom of this frame is presented in

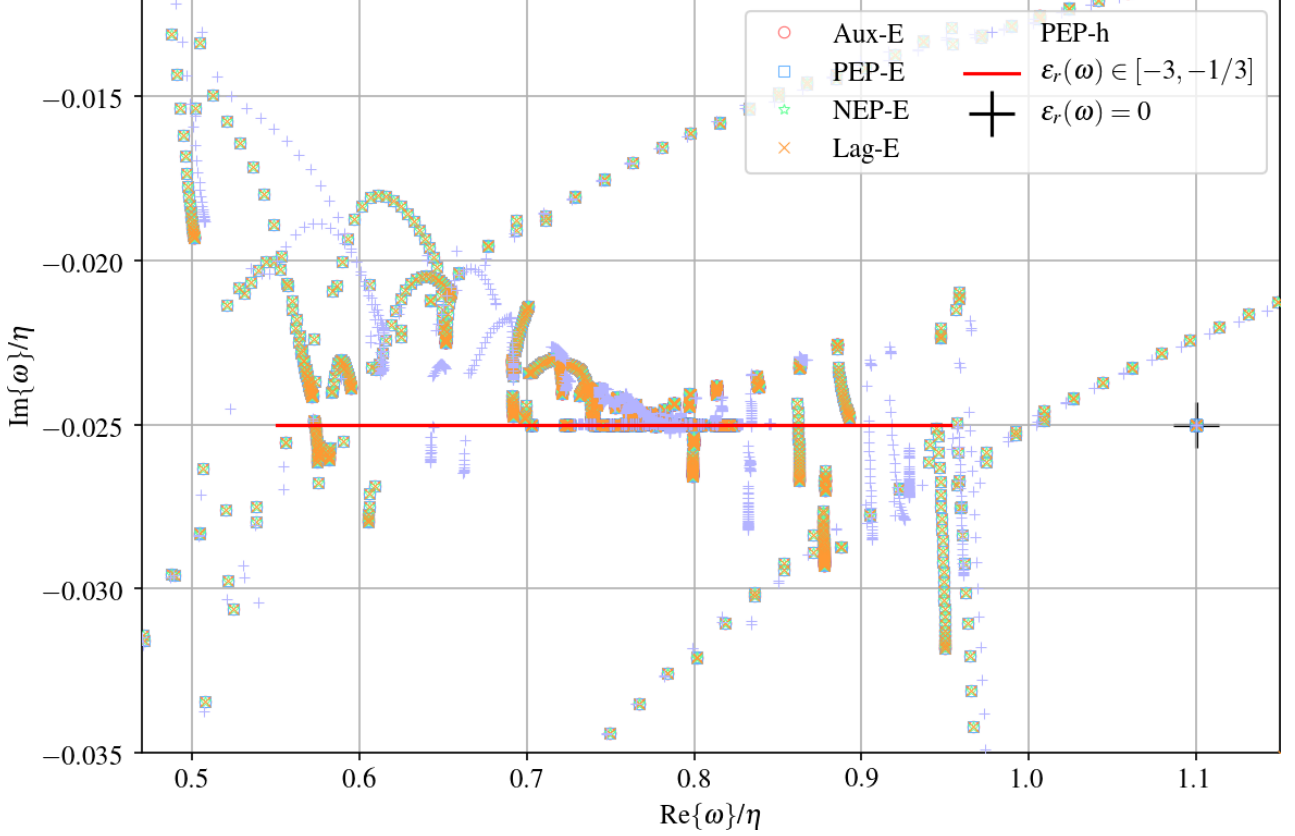


Figure 5: Eigenvalues in the complex plane. Zoom in the black rectangle depicted in Fig. 4.

Fig. 5.

5.4 Corner modes

In recent works [44, 45], variational formulations of the Helmholtz equation with sign changing coefficients has drawn a lot of attention in both direct [46] and spectral problems [47]. The sesquilinear form involving the sign-changing coefficient becomes non coercive and one cannot use the Lax-Milgram theorem to establish well-posedness. In the direct problem, with a real and fixed frequency, the problem exists but it is hidden by the simple fact that most of physical problems are dissipative (*i.e.* the real-part changing coefficient has a non vanishing imaginary part). However, in spectral problems with *complex frequencies*, there exist regions of the complex plane of frequencies for which the *sign-changing coefficient is purely real*.

One important starting point is that it is possible to foresee [47] the critical complex frequencies: Given θ , one of the internal geometric angle of the polygonal object whose permittivity exhibits a negative real part, the problem is ill-posed for:

$$\varepsilon_{r,2} \in [-I_\theta, -1/I_\theta], \text{ where } I_\theta = \max\left(\frac{2\pi - \theta}{\theta}, \frac{\theta}{2\pi - \theta}\right). \quad (26)$$

In this case, singularities appear at the corners and the expected corner modes are becoming more and more oscillating in the close vicinity of the corner. These solutions are no longer of finite energy, so in the functional frame of classical Galerkin FE used here, these modes known as “black-hole waves” cannot be represented. It is interesting to note that corner modes

correspond to continuous spectrum just as free-space. In this problem, the free-space continuous spectrum is handled (and discretized) using the PMLs. Recently, PMLs for corners [45] have been introduced.

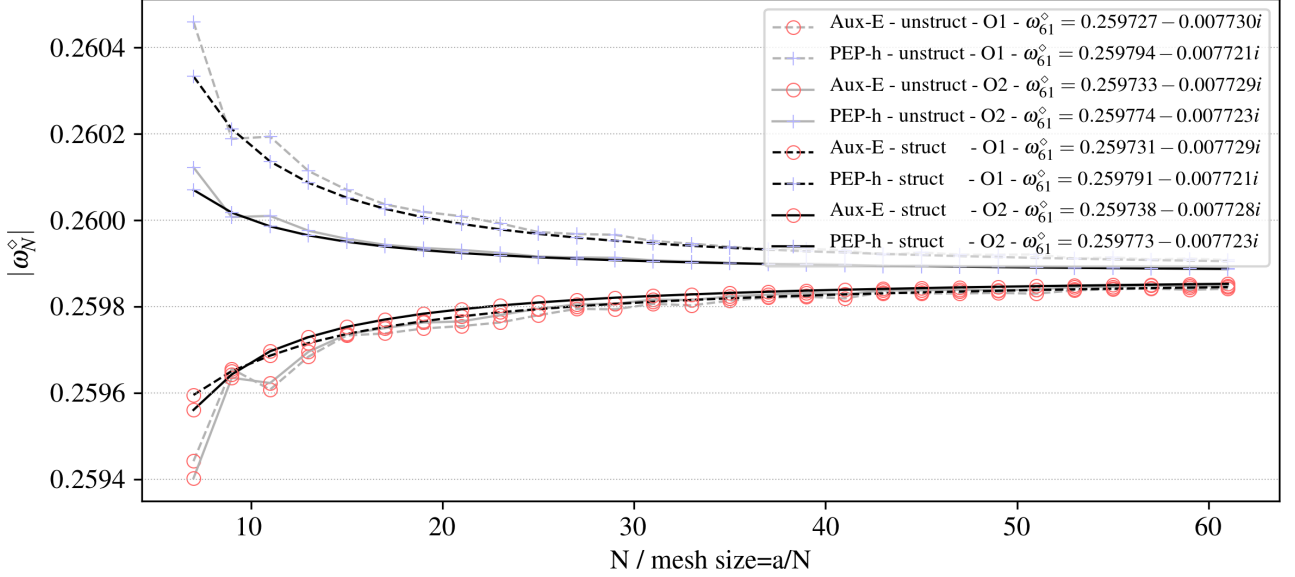


Figure 6: Convergence of the modulus of the eigenvalue ω^\diamond as function of the mesh refinement for the Aux-E and PEP-h formulation, for both unstructured and structured meshes, for first and second interpolation orders. The value of ω^\diamond for $N = 61$ is given in the legend for each case.

For the present dispersive rod consisting of $\pi/2$ angles, the critical interval is $[-3, -1/3]$. Again, the Drude relative permittivity studied here is lossy, so the issue is not critical on the line of real frequencies when tackling direct problems. Heuristically, the rapid oscillations of the field around the corners are damped sufficiently fast. However, when applying the Drude model to complex frequencies, it turns out that the quadratic equation $\varepsilon_{r,2}(\omega_c) = \kappa$ has one root ω_c in the quarter complex plane of interest for all $\kappa \in [-3, -1/3]$: $\omega_c = -i\gamma_d/2 + \sqrt{\gamma_d^2/4 + \omega_d^2/(1 - \kappa)}$. The red segment in Figs. (4,5) shows the locus of ω_c as κ spans $[-3, -1/3]$.

5.5 Convergence

In other words, all the modes eigenvalues around this segment are polluted by the presence of the corner modes. This explains the shift between the edge (electric here) discretizations and the nodal (magnetic) one: They both fail to capture the corner effect in a different manner. Indeed, in the (in-plane) edge case, the relevant unknowns associated with the corner are the circulation of the field along the two adjacent edges discretizing the corner, whereas in the (out-of-plane) nodal case, there is an unknown exactly on the corner. As moving closer to the critical interval, eigenvectors tend to look like four weighted hot spots around each corner, discretized differently which causes the discrepancy highlighted in Fig. 5. The correct way to address the problem is to take into account the corner modes and a rigorous approach is set up in Ref. [45] using a special kind of PML dedicated to corners.

When away from the critical interval, it is legitimate to question the convergence of the eigenvalues. Let us focus on one eigenvalue in particular, the lowest (fundamental) eigenfrequency for $\alpha = 3\pi/(4a)$, denoted ω^\diamond . It corresponds to the first grating dispersion line shown in

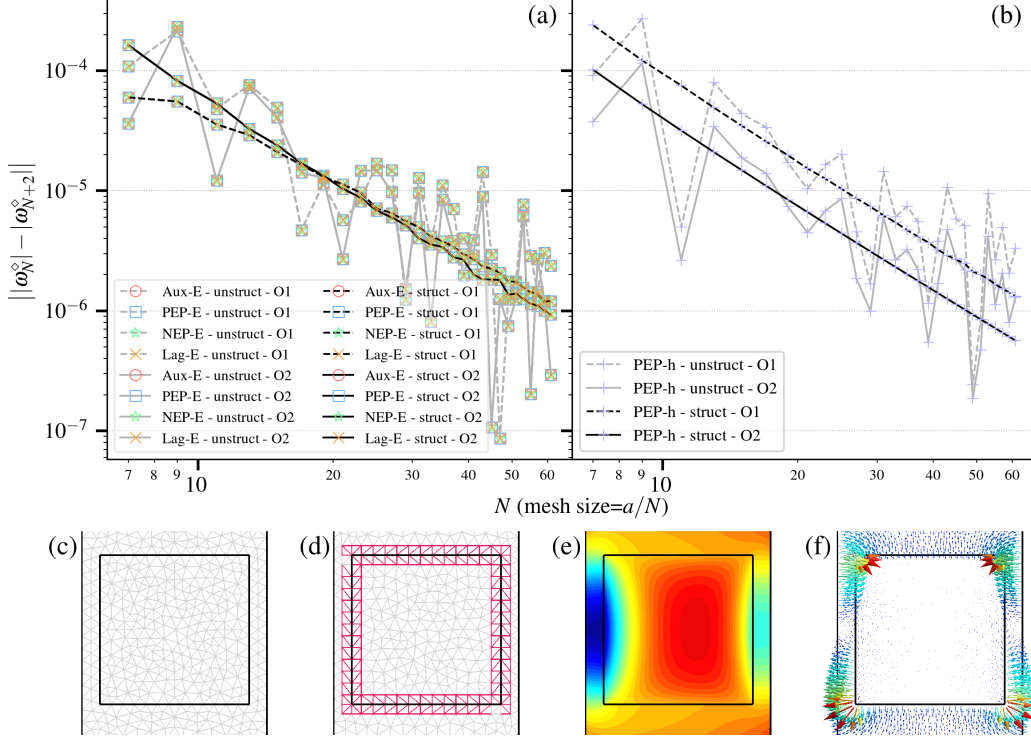


Figure 7: Convergence of an eigenvalue of the first branch for $\alpha = 3\pi/(4a)$ as a function of the mesh size parametrized by N . (a) Results for the electric field formulations (Aux-E, PEP-E, NEP-E, Lag-E using edge elements) for interpolation orders 1 (dashed lines) and 2 (solid lines), and the two types of mesh, unstructured (gray lines) and structured (dark lines) around the sign-changing material. (b) Results for the magnetic field formulation (PEP-h using nodal elements) for interpolation orders 1 (dashed line) and 2 (solid line), and the two types of mesh, unstructured (gray lines) and structured (dark lines) around the sign-changing dispersive material. (c) Unstructured mesh sample used for the convergence depicted in gray lines in (a-b). (d) Structured mesh sample used for the convergence depicted in dark lines in (a-b). (e) Real part of the out-of-plane component h^\diamond of the mode corresponding to ω^\diamond (arbitrary units). (f) Real part of the in plane vector mode profile \mathbf{E}^\diamond corresponding to ω^\diamond (arbitrary units).

Figs. 3(a). Figure 6 shows the value of the modulus of ω^\diamond as a function of the mesh refinement. For 61 mesh elements per period, 5 significant digits are found on the real part and 6 on the imaginary part, as shown in the legend. The convergence rate of this eigenvalue with the mesh refinement is shown in Figs. 7(a-b). The numerical value of this eigenfrequency for a mesh size parametrized by N as described previously is denoted ω_N^\diamond and the quantity $||\omega_N^\diamond - \omega_{N-2}^\diamond||$ is represented as a function of N , from $N = 7$ to $N = 60$ (that is 60 mesh elements per period) for two different interpolation orders 1 and 2. All electric (edge) formulations are represented in Fig. 7(a) while the magnetic (nodal) one is shown in Fig. 7(b). The different markers of the figure represent the formulation used with the same shape code as in previous figures. The line style represents the interpolation order (dashed for order 1 and solid for order 2). The line color represents the type of mesh used, which has not been discussed yet. For now, we only mentioned the classical unstructured Delaunay mesh type (see lines in gray color in Figs. 7(a)-(b)). The corresponding modes profiles h^\diamond (obtained with nodal elements and the PEP-h approach) and \mathbf{E}^\diamond (obtained with edge elements and the NEP-E approach) are depicted in Fig. 7(e) and

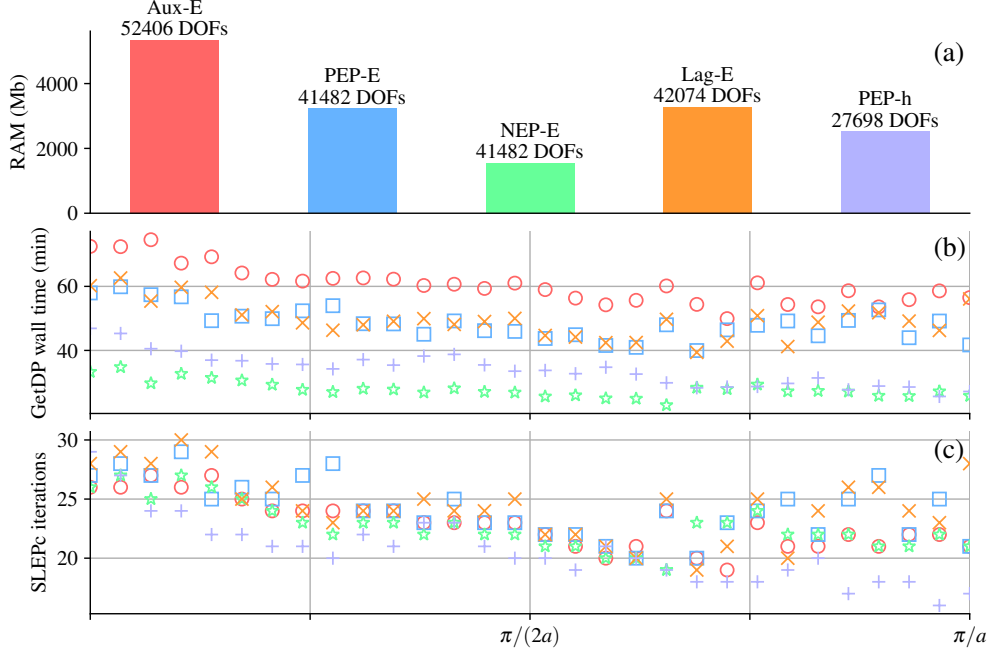


Figure 8: Computation time (b), memory requirements (a) and number of SLEPc iterations (c) to obtain the dispersion curves for the various presented approaches shown in Fig. 3 (Intel Xeon 2,7GHz processors).

Fig. 7(f) respectively. It is clear from this last figure that the hot spots at the corners play an important role in the convergence, even though ω^\diamond is away from the critical interval.

It is first important to note in Fig. 7(a) that the eigenvalues ω_N^\diamond seem identical irrespectively of the electric field formulation, in spite of the very different treatment of the non-linearity (except for the PEP-E and NEP-E which are twin approaches).

The second noticeable aspect is that the convergence is erratic for all approaches, scalar one included, irrespectively of the interpolation order with an unstructured mesh. In the vector case, increasing the interpolation order even seems to make things worse.

This chaotic behavior has been observed, again in the frame of corner issues and sign changing coefficients [45]. In the literature, it is recommended to use a mesh respecting particular symmetry properties around the sign-changing material for retrieving a better convergent behavior. This mesh has been implemented and the very same convergence study is presented in Figs. 7(a-b) with the same graphical conventions as above, but in black lines. It is very clear from the figure that the convergence is much more smooth than with the unstructured mesh : two straight (one for each interpolation order, see Fig. 7(b)) lines are obtained in the nodal case whereas those obtained for the edge elements (see black lines in Fig. 7(b)) are a slightly more bumpy, but much less than their unstructured counterparts. These results are consistent with those in [45].

Note that it is expected to find a change of slope due in the convergence [34] to the increased polynomial order. The convergence rate seems to be a bit higher for second interpolation order for edge elements whereas, for nodal elements, the two black lines are strictly parallel.

Table 2: A synthetic view of strengths and weakness of all the approaches.

Approach	Advantage	Limitation
Aux-E	<ul style="list-style-type: none"> • Physical linearization • Low polynomial order (2) • Easy to extend to several materials with more poles 	<ul style="list-style-type: none"> • System size • Speed
PEP-E	<ul style="list-style-type: none"> • Smallest system size 	<ul style="list-style-type: none"> • Tedious to generalize • Polynomial order can increase rapidly with several materials
NEP-E	<ul style="list-style-type: none"> • Smallest system size • Smallest memory requirements • Shortest runtime • Ease of implementation of the formulation 	<ul style="list-style-type: none"> • Stability and convergence with several materials with more poles?
Lag-E	<ul style="list-style-type: none"> • Domain by domain formulation with extra boundary unknowns • Low polynomial order 	<ul style="list-style-type: none"> • Extra boundary unknowns
PEP-h	<ul style="list-style-type: none"> • For comparison purposes, especially around the critical interval 	

5.6 Computation time and memory requirements

Some computation details are given for most time consuming simulations presented in this paper used to produce Figs. (3-5) with $N = 15$ and first order interpolation on a machine powered by Intel Xeon 2,7GHz processors. First, the RAM memory used is linked with both the system size and the SLEPc solver used. The most memory and time consuming approach is the auxiliary field one. The extra volume unknowns increase the system size by one third compared to the PEP/NEP-E approaches as shown in Fig. 8. Note that there is one single auxiliary field in this Drude case. We also stress that the approach using SLEPc non-linear rational NLEIGS solver is the fastest for this problem, even faster than the polynomial one (an average of 28 minutes per value of α for the NEP-E approach against 49 minutes for its twin NEP-E and 60 minutes for the Aux-E approach, see Fig. 8).

6 Conclusion

In this paper, several approaches aimed at linearizing the eigenvalue problem arising from the consideration of frequency-dispersion in electromagnetic structures have been introduced, implemented and discussed. The relative permittivity was considered under the form of a rational function of the eigenvalue with arbitrary degrees for the denominator and numerator. Five formulations were derived in the frame of a typical multi-domain problem exhibiting several key features in electromagnetism: The mono-dimensional grating is a quasi-periodic problem with PMLs. This is a 2D problem quite representative of 3D situations since the physics is as rich as in 3D (plasmons) and the vector case with edge elements is solved. We take advantage of the performance and versatility of the SLEPc library interfaced with the flexible GetDP Finite Element GNU software.

The first four formulations of the 2D problem concern the vector case and the choice of unknown is the electric field. First (Aux-E), physical auxiliary field(s) allow a linearization

of the problem by extending Maxwell’s operator, adding unknowns in the dispersive domains solely. The final polynomial EVP is quadratic. Second, writing the Maxwell problem under its variational form brings out immediately a polynomial (PEP-E) or rational (NEP-E) eigenvalue problem. An alternative consists in dealing with the rational function under the strong form of the problem and making the use of Lagrange multipliers (Lag-E) to deal with the non-classical boundary terms arising. The advantage of this approach is to keep the order of the polynomial EVP as low as the highest degree of all the denominator’s permittivity functions. Finally, for comparison, the polynomial approach is given for the scalar version of same polarization case using the magnetic field (PEP-h).

We obtain a perfect numerical agreement between all the electric field approaches in spite of the fact that they rely on very different linearization strategies. As for the magnetic one, when away from the critical interval inherent to the presence of the sign changing permittivity and sharp angles, the agreement still holds. As for this critical interval associated with solutions of infinite energy, they cannot be captured with the classical finite element scheme. Specific PMLs should be adapted. However, away from the critical interval, for instance for the fundamental mode of the grating, a smooth convergence is obtained when using a specific locally structured and symmetric mesh.

To conclude on the main features of the presented approaches, the auxiliary fields (Aux-E) allow for a physical linearization that is extremely valuable, since irrespectively of the number of poles of the permittivity function, a quadratic EVP is obtained. In return, the final system is much larger than with all other approaches. The approach using Lagrange multipliers (Lag-E) deserves some attention since the polynomial order will not blow with an increased number of dispersive materials. In this test case with a simple Drude model, the SLEPc rational NLEIGS solver used in the NEP-E approach gives the best results in terms of ease of implementation, speed, and memory occupation.

Direct perspectives of this work are of course to extend and verify the identified behavior to the 3D case with more complex permittivity dispersion relations. Considering more poles to the permittivity functions also means more complex frequencies lines leading to the critical interval. Inevitably, the special PML for corners should be extended to the 3D case and carefully studied in a future work.

Acknowledgements

The work was partly supported by the French National Agency for Research (ANR) under the project “Resonance” (ANR-16-CE24-0013). The authors acknowledge the members of the project “Resonance” for fruitful discussions. C. Campos and J. E. Roman were supported by the Spanish Agencia Estatal de Investigación (AEI) under project SLEPc-HS (TIN2016-75985-P), which includes European Commission ERDF funds.

Finally, the authors address special thanks to Anne-Sophie Bonnet Ben-Dhia and Camille Carvalho from INRIA (POEMS) for their motivating remarks and insights.

References

- [1] J. D. Jackson, *Classical electrodynamics*. John Wiley & Sons, 2007.

- [2] P. G. Etchegoin, E. Le Ru, and M. Meyer, “An analytic model for the optical properties of gold,” *The Journal of Chemical Physics*, vol. 125, no. 16, p. 164705, 2006.
- [3] M. Garcia-Vergara, G. Demésy, and F. Zolla, “Extracting an accurate model for permittivity from experimental data: hunting complex poles from the real line,” *Optics Letters*, vol. 42, no. 6, pp. 1145–1148, 2017.
- [4] C. Sauvan, J.-P. Hugonin, I. Maksymov, and P. Lalanne, “Theory of the spontaneous optical emission of nanosize photonic and plasmon resonators,” *Physical Review Letters*, vol. 110, no. 23, p. 237401, 2013.
- [5] B. Vial, M. Commandré, G. Demésy, A. Nicolet, F. Zolla, F. Bedu, H. Dallaporta, S. Tisserand, and L. Roux, “Transmission enhancement through square coaxial aperture arrays in metallic film: when leaky modes filter infrared light for multispectral imaging,” *Opt. Lett.*, vol. 39, pp. 4723–4726, Aug 2014.
- [6] W. Yan, R. Faggiani, and P. Lalanne, “Rigorous modal analysis of plasmonic nanoresonators,” *arXiv preprint arXiv:1711.05011*, 2017.
- [7] P. Lalanne, W. Yan, K. Vynck, C. Sauvan, and J.-P. Hugonin, “Light interaction with photonic and plasmonic resonances,” *arXiv preprint arXiv:1705.02433*, 2017.
- [8] H. van der Lem, A. Tip, and A. Moroz, “Band structure of absorptive two-dimensional photonic crystals,” *JOSA B*, vol. 20, no. 6, pp. 1334–1341, 2003.
- [9] Q. Bai, M. Perrin, C. Sauvan, J.-P. Hugonin, and P. Lalanne, “Efficient and intuitive method for the analysis of light scattering by a resonant nanostructure,” *Optics express*, vol. 21, no. 22, pp. 27371–27382, 2013.
- [10] O. Toader and S. John, “Photonic band gap enhancement in frequency-dependent dielectrics,” *Physical Review E*, vol. 70, no. 4, p. 046605, 2004.
- [11] G. Alagappan and A. Deinega, “Optical modes of a dispersive periodic nanostructure,” *Progress In Electromagnetics Research B*, vol. 52, pp. 1–18, 2013.
- [12] T. Weiss, M. Mesch, M. Schäferling, H. Giessen, W. Langbein, and E. Muljarov, “From dark to bright: first-order perturbation theory with analytical mode normalization for plasmonic nanoantenna arrays applied to refractive index sensing,” *Physical review letters*, vol. 116, no. 23, p. 237401, 2016.
- [13] J. Zimmerling, L. Wei, P. Urbach, and R. Remis, “A Lanczos model-order reduction technique to efficiently simulate electromagnetic wave propagation in dispersive media,” *Journal of Computational Physics*, vol. 315, pp. 348–362, 2016.
- [14] J. Zimmerling, L. Wei, P. Urbach, and R. Remis, “Efficient computation of the spontaneous decay rate of arbitrarily shaped 3D nanosized resonators: a Krylov model-order reduction approach,” *Applied Physics A*, vol. 122, no. 3, p. 158, 2016.
- [15] D. A. Powell, “Resonant dynamics of arbitrarily shaped meta-atoms,” *Physical Review B*, vol. 90, no. 7, p. 075108, 2014.

- [16] D. A. Powell, “Interference between the modes of an all-dielectric meta-atom,” *Physical Review Applied*, vol. 7, no. 3, p. 034006, 2017.
- [17] F. Tisseur and K. Meerbergen, “The quadratic eigenvalue problem,” *SIAM Review*, vol. 43, no. 2, pp. 235–286, 2001.
- [18] D. S. Mackey, N. Mackey, and F. Tisseur, “Polynomial eigenvalue problems: theory, computation, and structure,” in *Numerical Algebra, Matrix Theory, Differential-Algebraic Equations and Control Theory* (P. Benner *et al.*, eds.), pp. 319–348, 2015.
- [19] S. Güttel and F. Tisseur, “The nonlinear eigenvalue problem,” *Acta Numerica*, vol. 26, pp. 1–94, 2017.
- [20] V. Hernandez, J. E. Roman, and V. Vidal, “SLEPc: A scalable and flexible toolkit for the solution of eigenvalue problems,” *ACM Transactions on Mathematical Software*, vol. 31, no. 3, pp. 351–362, 2005.
- [21] Y. Brûlé, B. Gralak, and G. Demésy, “Calculation and analysis of the complex band structure of dispersive and dissipative two-dimensional photonic crystals,” *JOSA B*, vol. 33, no. 4, pp. 691–702, 2016.
- [22] B. Vial, F. Zolla, A. Nicolet, and M. Commandré, “Quasimodal expansion of electromagnetic fields in open two-dimensional structures,” *Physical Review A*, vol. 89, p. 023829, Feb. 2014.
- [23] A. Bermúdez, L. Hervella-Nieto, A. Prieto, R. Rodri, *et al.*, “An optimal Perfectly Matched Layer with unbounded absorbing function for time-harmonic acoustic scattering problems,” *Journal of Computational Physics*, vol. 223, no. 2, pp. 469–488, 2007.
- [24] A. Modave, E. Delhez, and C. Geuzaine, “Optimizing Perfectly Matched Layers in discrete contexts,” *International Journal for Numerical Methods in Engineering*, vol. 99, no. 6, pp. 410–437, 2014.
- [25] F. Zolla, G. Renversez, A. Nicolet, B. Kuhlmeier, S. Guenneau, and D. Felbacq, *Foundations of photonic crystal fibres*. World Scientific, 2005.
- [26] A. Tip, “Linear absorptive dielectrics,” *Physical Review A*, vol. 57, no. 6, p. 4818, 1998.
- [27] B. Gralak and A. Tip, “Macroscopic Maxwell’s equations and negative index materials,” *Journal of Mathematical Physics*, vol. 51, no. 5, p. 052902, 2010.
- [28] A. Tip, “Some mathematical properties of Maxwell’s equations for macroscopic dielectrics,” *Journal of Mathematical Physics*, vol. 47, no. 1, p. 012902, 2006.
- [29] A. Raman and S. Fan, “Photonic band structure of dispersive metamaterials formulated as a Hermitian eigenvalue problem,” *Physical Review Letters*, vol. 104, no. 8, p. 087401, 2010.
- [30] A. Taflov and S. C. Hagness, *Computational electrodynamics: the finite-difference time-domain method*. Artech house, 2005.

- [31] A. Nicolet, S. Guenneau, C. Geuzaine, and F. Zolla, “Modelling of electromagnetic waves in periodic media with finite elements,” *Journal of Computational and Applied Mathematics*, vol. 168, no. 1, pp. 321–329, 2004.
- [32] C. Geuzaine and J.-F. Remacle, “Gmsh: a three-dimensional finite element mesh generator with built-in pre- and post-processing facilities,” *International Journal for Numerical Methods in Engineering*, vol. 79, no. 11, pp. 1309–1331, 2009.
- [33] J. Webb and B. Forgahani, “Hierarchical scalar and vector tetrahedra,” *IEEE Transactions on Magnetics*, vol. 29, no. 2, pp. 1495–1498, 1993.
- [34] C. Geuzaine, B. Meys, P. Dular, and W. Legros, “Convergence of high order curl-conforming finite elements [for EM field calculations],” *IEEE Transactions on Magnetics*, vol. 35, no. 3, pp. 1442–1445, 1999.
- [35] P. Dular, C. Geuzaine, F. Henrotte, and W. Legros, “A general environment for the treatment of discrete problems and its application to the finite element method,” *IEEE Transactions on Magnetics*, vol. 34, no. 5, pp. 3395–3398, 1998.
- [36] D. Lu, Y. Su, and Z. Bai, “Stability analysis of the two-level orthogonal Arnoldi procedure,” *SIAM Journal on Matrix Analysis and Applications*, vol. 37, no. 1, pp. 195–214, 2016.
- [37] C. Campos and J. E. Roman, “Parallel Krylov solvers for the polynomial eigenvalue problem in SLEPc,” *SIAM Journal on Scientific Computing*, vol. 38, no. 5, pp. S385–S411, 2016.
- [38] C. Campos and J. E. Roman, “NEP: a module for the parallel solution of nonlinear eigenvalue problems in SLEPc.” In preparation, 2018.
- [39] S. Güttel, R. van Beeumen, K. Meerbergen, and W. Michiels, “NLEIGS: A class of fully rational Krylov methods for nonlinear eigenvalue problems,” *SIAM Journal on Scientific Computing*, vol. 36, no. 6, pp. A2842–A2864, 2014.
- [40] Y. Brûlé, B. Gralak, and G. Demézy, “Calculation and analysis of the complex band structure of dispersive and dissipative two-dimensional photonic crystals,” *JOSA B*, vol. 33, no. 4, pp. 691–702, 2016.
- [41] P. Lalanne, J. Rodier, and J. Hugonin, “Surface plasmons of metallic surfaces perforated by nanohole arrays,” *Journal of Optics A: Pure and Applied Optics*, vol. 7, no. 8, p. 422, 2005.
- [42] P. Lalanne, J. P. Hugonin, and P. Chavel, “Optical properties of deep lamellar gratings: a coupled Bloch-mode insight,” *Journal of Lightwave Technology*, vol. 24, no. 6, pp. 2442–2449, 2006.
- [43] G. Schider, J. Krenn, A. Hohenau, H. Ditlbacher, A. Leitner, F. Aussenegg, W. Schaich, I. Puscasu, B. Monacelli, and G. Boreman, “Plasmon dispersion relation of Au and Ag nanowires,” *Physical Review B*, vol. 68, no. 15, p. 155427, 2003.
- [44] L. Chesnel and P. Ciarlet, “T-coercivity and continuous Galerkin methods: application to transmission problems with sign changing coefficients,” *Numerische Mathematik*, vol. 124, no. 1, pp. 1–29, 2013.

- [45] C. Carvalho, *Étude mathématique et numérique de structures plasmoniques avec coins*. PhD thesis, ENSTA ParisTech, 2015.
- [46] A.-S. Bonnet-Ben Dhia, C. Carvalho, and P. Ciarlet, “Mesh requirements for the finite element approximation of problems with sign-changing coefficients,” *Numerische Mathematik*, Oct 2017.
- [47] C. Carvalho, L. Chesnel, and P. Ciarlet, “Eigenvalue problems with sign-changing coefficients,” *Comptes Rendus Mathématique*, 2017.